An Adaptive and Fast CFAR Algorithm Based on Automatic Censoring for Target Detection in High-Resolution SAR Images

Gui Gao, Li Liu, Lingjun Zhao, Gongtao Shi, and Gangyao Kuang

***Abstract*—An adaptive and fast constant false alarm rate (CFAR) algorithm based on automatic censoring (AC) is proposed for target detection in high-resolution synthetic aperture radar (SAR) images. First, an adaptive global threshold is selected to obtain an index matrix which labels whether each pixel of the image is a potential target pixel or not. Second, by using the index matrix, the clutter environment can be determined adaptively to prescreen the clutter pixels in the sliding window used for detecting. The G^0 distribution, which can model multilook SAR images within an extensive range of degree of homogeneity, is adopted as the statistical model of clutter in this paper. With the introduction of AC, the proposed algorithm gains good CFAR detection performance for homogeneous regions, clutter edge, and multitarget situations. Meanwhile, the corresponding fast algorithm greatly reduces the computational load. Finally, target clustering is implemented to obtain more accurate target regions. According to the theoretical performance analysis and the experiment results of typical real SAR images, the proposed algorithm is shown to be of good performance and strong practicability.**

***Index Terms*—Constant false alarm rate (CFAR), synthetic aperture radar (SAR), target detection.**

I. Introduction

With the increasing volume of image data which are collected from air- and spaceborne synthetic aperture radar (SAR) sensors, it is becoming increasingly desirable to develop the techniques for SAR image interpretation. A task which is of particular importance for SAR image interpretation is to recognize vehicle targets or groups of targets in background clutter [1]–[4]. As automatic detection is the first important step of an automatic target recognition (ATR) system, fast detection of targets, such as tanks, armored personnel carriers, trucks, and howitzers, can afford to meet the expanding requirements of intelligence, surveillance, and reconnaissance.

Manuscript received October 28, 2007; revised June 14, 2008. First published December 12, 2008; current version published May 22, 2009. This work was supported by the National Natural Science Foundation of China under Projects 60772045 and 40801179.

G. Gao is with the School of Electronics Science and Engineering, National University of Defense Technology, Changsha 410073, China (e-mail: dellar@126.com).

L. Liu, L. Zhao, and G. Shi are with the National University of Defense Technology, Changsha 410073, China (e-mail: feiyunlyi@hotmail.com; nudtzlj@163.com; shigongtao@si-na.com).

G. Kuang is with the Remote Sensing Information Processing Laboratory, School of Electronic Science and Engineering, National University of Defense Technology, Changsha 410073, China (e-mail: kgyyeats@vip.sina.com).

Digital Object Identifier 10.1109/TGRS.2008.2006504

At the fist step of the whole SAR ATR system, target detection has great influence on the successive processing [5], [6]. So far, there are many algorithms of target detection for SAR image available in literature. Among these algorithms, constant false alarm rate (CFAR) detection, because of its characteristics of simple computation, constant false alarm probability, adaptive threshold, and fast detection of targets from complex background, has been extensively studied [7], [8] and even applied in several SAR ATR systems [9], [10].

The commonly used CFAR detection algorithms include [6], [7], [11], [21] the cell averaging CFAR (CA-CFAR), greatest of CFAR (GO-CFAR), smallest of CFAR (SO-CFAR), order statistic CFAR (OS-CFAR), etc. The CA-CFAR (the two-parameter CFAR algorithm proposed by Lincoln Laboratory is actually a CA-CFAR technique based on the assumption of Gaussian background [9], [22]) technique works well in situations where a single target is present in locally homogeneous clutter. In the presence of heterogeneous environment (including the clutter edge and multitarget situations), however, the performance of the CA-CFAR detector degrades rapidly [6]. The OS-CFAR algorithm is designed to overcome the problem of the loss in detection performance suffered by the CA-CFAR, when interfering targets are in the background cells and clutter statistics estimation is corrupted. Therefore, it has significant advantage when detecting targets in multitarget situations. However, in homogenous scene, the OS-CFAR algorithm performs worse than the CA-CFAR algorithm [6]. Furthermore, the optimal statistic is usually obtained by experience instead of by theory. Moreover, the operation of ordering will inevitably increase the computational load. The GO-CFAR algorithm provides good detection performance in clutter edge situations. Compared with the CA-CFAR algorithm, its detection performance degrades in homogeneous clutter scene because of the loss of the correlated information among pixels. The SO-CFAR algorithm can achieve better performance in multitarget situations. In clutter edge situations, however, it produces more false alarms than the CA-CFAR algorithm does because the corresponding detection threshold is lower.

The CA-CFAR, OS-CFAR, GO-CFAR, SO-CFAR, etc. are the basic CFAR detection algorithms [6], [11], [12], [21]. Each of them has its advantages, disadvantages, and situations of potential application. No single detector performs well in all kinds of scenes. If we introduce a methodology to select these basic CFAR detectors mentioned earlier, adaptively according to the position of the tested pixel, there will be a significant

improvement in detection performance. Based on the consideration, current research works on CFAR algorithms have focused on developing adaptive CFAR algorithms [12].

Many researchers have attempted to design adaptive CFAR algorithms. The variability index CFAR (VI-CFAR) proposed by Smith and Varshney [12], [13] is a representative one. The VI-CFAR processor provides CFAR performance in both homogeneous and nonhomogeneous situations of clutter. Based on the VI-CFAR, Huang *et al.* propose the region classification CFAR (RC-CFAR) [14]. According to [15], the RC-CFAR subdivides the reference cell into four parts so that the number of target samples in each part becomes too less; thus, it is less credible to judge whether the environment is nonhomogeneous. Drawing the inspiration from the VI-CFAR, Farrouki and Barkat present the ordered data variability index automatic censoring (AC) CFAR detector to realize adaptive target detection in complex background [16]. Assuming the Weibull clutter background, Bisceglie proposes a solid-stencil CFAR detector (the so-called the Bisceglie algorithm [7], [17]), including comprehensive procedures such as sorting, censoring, etc. The similar idea of censoring is proposed by Rickard and Dillard [18]. It is reported [7], [17] that the Bisceglie algorithm is suitable for the clutter of location-scale type (LS-type). LS-type clutter can be regarded as the regularization of the clutter distribution with two parameters. The experiment results [7], [17] show that the algorithm performs well in both homogeneous and nonhomogeneous environments. It is reasonable to say that the Bisceglie algorithm is an excellent CFAR detection algorithm. Further investigations can be carried out on the clutter models, automatic selection of the censoring depth, selection of the sliding-window type, etc. Moreover, an innovative CFAR algorithm called cell averaging statistic Hofele (CASH) CFAR is introduced in [21]. The advantage of the CASH CFAR algorithm is that it avoids alternate covering and aggregation of objects. The required processing power of the CASH CFAR algorithm is also significantly less than that of the OS- and cell averaging ordered statistic CFAR algorithms [21]. Furthermore, a notable CFAR algorithm [8] (simply mentioned as the Salazar algorithm in this paper) has been presented by Salazar, which chooses the β' (beta-prime) distribution [19] as the statistical model of background clutter in a single-look SAR image. The main principle of the algorithm is described as follows: The β' distribution is proper to model clutter with widely varying degrees of homogeneity [19] [including homogeneous clutter, heterogeneous clutter edges, and multitarget situations (multitarget situations are equivalent to extremely heterogeneous clutter)]. Therefore, the CA-CFAR technique based on the β' distribution has the ability of keeping CFAR [8]. The algorithm does have CFAR characteristic for detecting target in homogeneous clutter, clutter edges, and multitarget situations. Moreover, because the contrast of the target pixels is larger than that of the surrounding clutter, the algorithm also offers higher detection probability in homogeneous clutter and clutter edges [8]. However, as for multitarget situations, the deficiency of the algorithm is that the CFAR threshold becomes large when the estimated clutter statistics are corrupted by interfering targets, which leads to a significantly reduced detection rate.

In this paper, an adaptive and fast CFAR algorithm based on AC is proposed for target detection in SAR image. The proposed algorithm is an improvement of the Salazar algorithm. Simultaneously, the corresponding fast algorithm is designed. This paper is organized as follows. In Section II, an introduction to the principles and the detailed flow of the algorithm are given. In Section III, the algorithm is described in detail. In Section IV, the corresponding fast algorithm is designed. Section V theoretically analyzes the performance of the presented algorithm. In Section VI, we provide the experimental results and the detection performance comparison of the proposed algorithm and other algorithms using typical real SAR data. The last section concludes this paper.

II. Principles and Detailed Flow of the Algorithm

A. Principles of Algorithm

The following suggestions can be derived from the algorithms mentioned earlier.

1) An indexing value is utilized in the VI-CFAR [12]–[14] to automatically judge the type of surrounding clutter of the test pixel to choose a proper detector, but the indexing value should be acquired adaptively instead of by experience.
2) A new way provided by the Bisceglie algorithm [7], [17] with additional procedures of prescreening and sorting can help to avoid the influence of interfering targets on the detection performance in multitarget situations.
3) The β' distribution adopted as the clutter model in the Salazar algorithm [8] can properly describe the homogeneous clutter, clutter edges, and multitarget situations, which makes it possible to obtain an integrative design for target detection algorithm in homogeneous clutter and clutter edges. Only target detection in multitarget situations should be considered separately.
4) By computing proper index values and deciding whether a clutter pixel in the sliding window belongs to an interfering target or not, we can censor all the interfering pixels. For the rest pixels, we perform the CA-CFAR algorithm.

The presented detection algorithm is designed based on the points mentioned earlier. As shown in Fig. 1, the whole detection process is summarized as follows. First, we select the square hollow-stencil sliding window, which is suitable for high-resolution SAR target detection [6]. During the process of the sliding window scanning the whole image, we consider the clutter area (clutter region) surrounding the test cell in the sliding window. It is assumed that there are N_C pixels in the area. Then, the clutter pixels that may belong to the interfering targets (we suppose there are D pixels censored, namely, the censoring depth is D) are censored by the index values that label the clutter pixels in the sliding window to be a potential pixel of interfering targets or not. Thus, the pixels that may not belong to the interfering targets are remained (there are $N_C - D$ pixels remained). The CA-CFAR technique is carried out on the rest $N_C - D$ pixels to yield the estimation of the parameters for the clutter model (the G^0 distribution). Moreover,

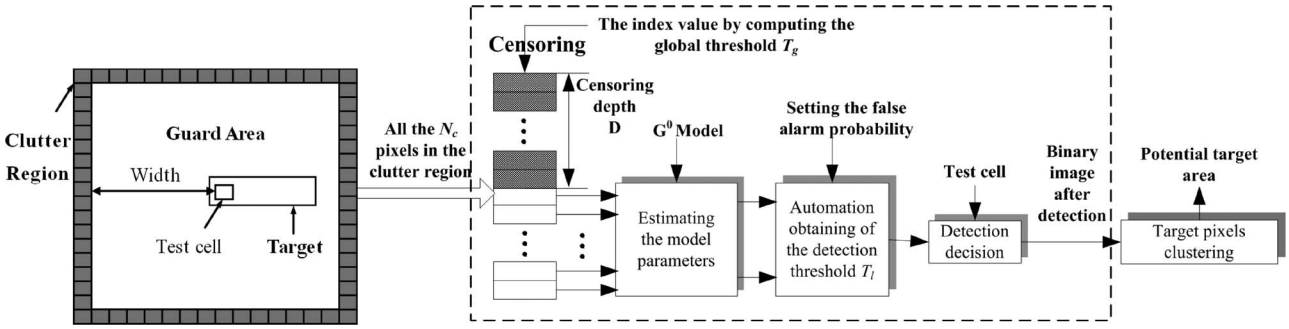

Fig. 1. Algorithm of target detection in this paper.

we compute the local detection threshold of the CFAR detector by setting the false alarm probability. Finally, we succeed in detecting targets by comparing the value of the test cell with the threshold. Simultaneously, because a small number of scatters in SAR images typically dominate the target's returns and, after detection, these bright peaks may not be connected as a region, the pixels in the binary image after CFAR operation have to be clustered. At last, the potential target region is obtained.

Some points need to be explained.

1) Although many statistical models of SAR images have been proposed (see [23]–[27]), the theoretical analysis and the experiment results of many typically real SAR scenes in literature [19] have confirmed that the G^0 distribution is suitable for modeling multilook clutter with widely varying degrees of homogeneity. The parameter estimation of the G^0 distribution is easy, and the computational complexity is low. Thus, we select the G^0 distribution to model the clutter region in local sliding window in this paper. The intensity form of the G^0 distribution, denoted byG_I^0, is given by [19]

$$f_{Z_I}(I) \sim G_I^0(\alpha,\gamma,n) = \frac{n^n \Gamma(n-\alpha) I^{n-1}}{\gamma^\alpha \Gamma(n)\Gamma(-\alpha)(\gamma+nI)^{n-\alpha}}, \quad -\alpha,\gamma,n,I>0 \quad (1)$$

where I is the intensity variable, n is the equivalent number of looks, α is the shape parameter, and γ is the scale parameter.

2) Generally speaking, targets have stronger backscattering than natural clutter; thus, the target pixels have higher gray value (abnormal point). However, the number of target pixels is much fewer than that of clutter pixels in a SAR image. Before performing target detection with the sliding window, a proper global threshold can be selected to scan the whole image to determine the target pixels. Pixels whose intensities are larger than the global threshold are considered as target pixels, and the index value is assigned with one; otherwise, the index value is assigned with zero. Therefore, an index matrix is obtained to automatically select the censoring depth for target detection.

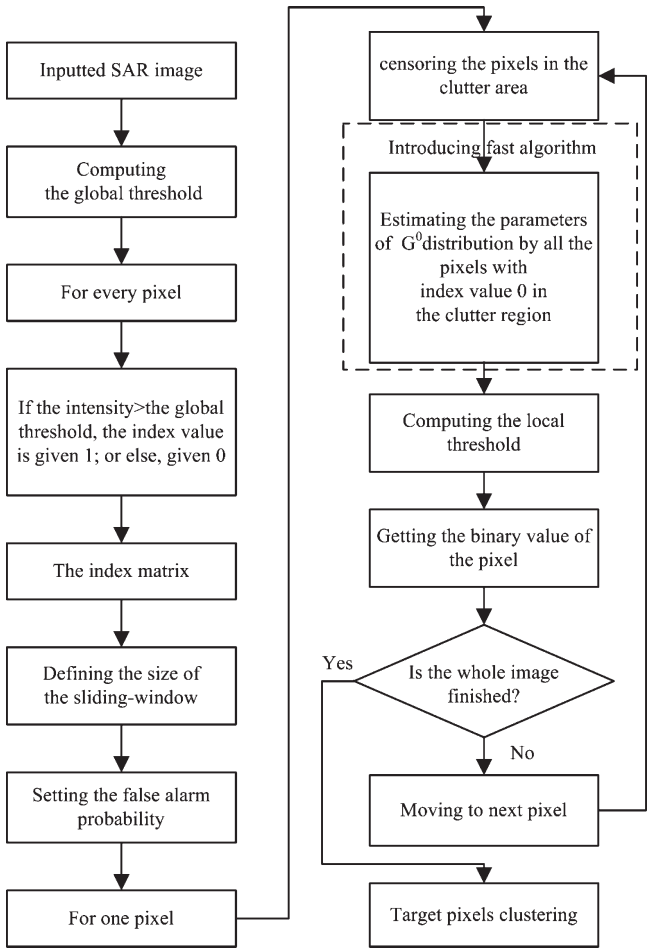

Fig. 2. Detailed flow of target detection algorithm in this paper.

B. Algorithm Details

To summarize, as shown in Fig. 2, the algorithm consists of the following steps.

Step 1) The global threshold of the input SAR image is computed.

Step 2) The index matrix is generated. For every pixel in the image, if it has an intensity value greater than the global threshold, its index value is one. Otherwise, its index value is zero.

Step 3) The size of target area, protected (guard) area, and background (clutter) area in the sliding window are

chosen according to the prior knowledge of the target size. The false alarm probability is initialized.

Step 4) The N_C clutter pixels in the sliding window of detection process are censored automatically by the index matrix. The clutter pixels that may be the pixels of interfering targets (suppose there are D pixels censored) are removed. Thus, $N_C - D$ pixels are left. Then, we estimate the parameters of the clutter model (the G^0 distribution) using the left $N_C - D$ pixels and compute the local detection threshold T_l.

Step 5) By comparing the intensity of the test cell with the local threshold, we obtain the binary value of the pixel.

Step 6) If it is the end of the whole input image, turn to Step 7). Otherwise, move on to the next pixel and repeat the process from Step 4).

Step 7) The detected target pixels in the binary image are clustered.

III. Algorithm Description

A. Computation of the Global Threshold T_g

Because the tailed part of the histogram of SAR image represents target pixels, T_g can be determined adaptively according to the histogram. Let I be the corresponding intensity random variable; under the condition that the confidence of being a target pixel is $1-\varphi$, T_g can be obtained from

$$P\{I > T_g\} = 1 - \varphi \tag{2}$$

where P is the probability, and $\varphi \in [0,1]$ is the empirical value that indicates the proportion of clutter pixels to the whole image, namely, the confidence of a pixel being a target pixel. φ is large in a large SAR image, approaching one. Furthermore, let F be the cumulative distribution function obtained from the histogram of the image under detection; (2) can be rewritten as

$$1 - F(T_g) = 1 - \varphi. \tag{3}$$

Then, T_g can be conveniently obtained from the histogram of the whole image by (3).

B. Index Matrix

Consider a SAR image of size $N \times M$, and let $I_{i,j}$ be the intensity of the pixel localized at the ith row and the jth column; we define the index value as $V_{i,j}$

$$V_{i,j} = \begin{cases} 1, & I_{i,j} > T_g \\ 0, & \text{other.} \end{cases} \tag{4}$$

Thus, the index matrix of the image is given by

$$\mathbf{V} = \{V_{i,j} | 1 \le i \le N; 1 \le j \le M\}. \tag{5}$$

C. Computation of the Local Threshold T_l of CFAR Detector

As shown in Fig. 1, in order to avoid the influence of the strongly backscattering parts of targets on the parameter estimation of the clutter distribution in the local sliding window, we select the square hollow-stencil sliding window centered at the test cell [9], [10]. The guard area exists to ensure that the clutter pixels are collected at some distance away from the test cell to prohibit target pixels from leaking into the background and corrupting clutter statistics estimation. Moreover, the pixels used to compute the clutter statistics are in a hollow square centered on the test cell. With this aim, the inner side length of the square should be larger than the expected size of the target, and the outer side length of the square is selected to make enough clutter pixels be included to estimate clutter statistics accurately.

The intensity distribution of the left $N_C - D$ clutter pixels in the sliding window after censoring is considered by (1). The left $N_C - D$ clutter pixels are used to compute the moment estimation of the parameters, leading to the following:

$$\hat{\alpha} = -1 - \frac{nE(I^2)}{nE(I^2) - (n+1)E^2(I)} \tag{6}$$

$$\hat{\gamma} = (-\hat{\alpha} - 1)E(I). \tag{7}$$

For a given value of the false alarm probability, denoted by p_{fa}, the corresponding local threshold T_l for the CFAR detector is obtained from

$$1 - p_{\text{fa}} = \int_0^{T_l} f_{Z_I}(I)\, dI. \tag{8}$$

As for the G_I^0 distribution, the aforementioned integral does not have an analytic expression. Local threshold T_l can be obtained by dichotomy (for details, see [20]).

For a single-look image, the G_I^0 distribution degrades to the β' distribution [19]

$$f_{Z_I}(I) = \frac{-\alpha\gamma^{-\alpha}}{(\gamma + I)^{1-\alpha}}, \qquad -\alpha, \gamma, I > 0 \tag{9}$$

(6) and (7) lead to the estimation of the parameters

$$\hat{\alpha} = -1 - \frac{E(I^2)}{E(I^2) - 2E^2(I)} \tag{10}$$

$$\hat{\gamma} = (-\hat{\alpha} - 1)E(I). \tag{11}$$

Similarly, for a given value of the false alarm probability p_{fa}, the corresponding local threshold T_l for the CFAR detector is obtained from (8)

$$T_l = \hat{\gamma}\left(p_{\text{fa}}^{1/\hat{\alpha}} - 1\right). \tag{12}$$

Accordingly, for the test cell with intensity I_0 in the sliding window, the target is detected according to the following

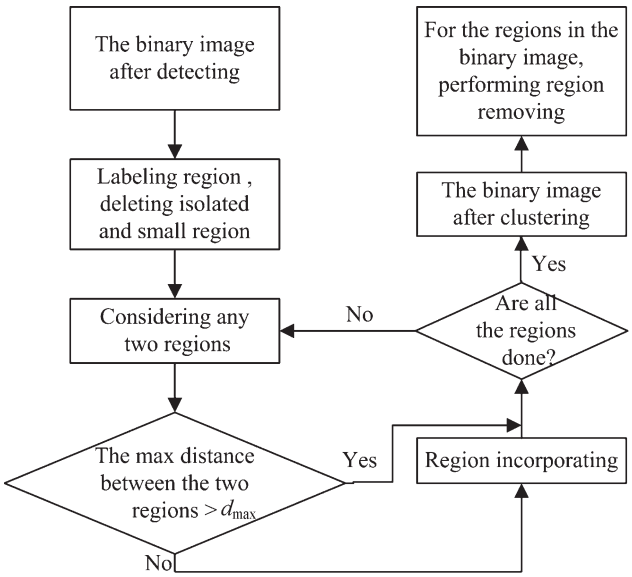

Fig. 3. Clustering flow of target pixels.

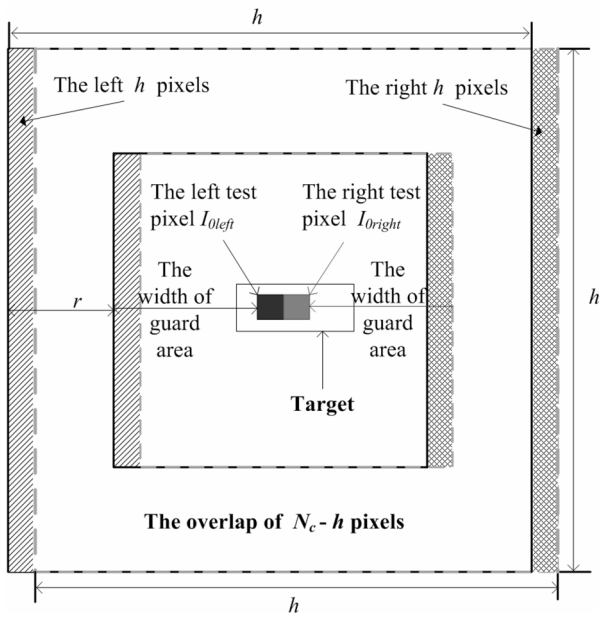

Fig. 4. Illustration of size for the sliding window.

decision rule:

$$I_0 \underset{H_0}{\overset{H_1}{\gtrless}} T_l \tag{13}$$

where H_1 is the hypothesis that the test cell is a target pixel, and H_0 is the hypothesis that the test cell is a clutter pixel. The local threshold T_l is adaptively obtained pixel by pixel.

D. Target Pixel Clustering

In high-resolution SAR images, a target, also mentioned as extended object, consists of many resolution cells. Because the reflection of a target surface may appear as fluctuation, the corresponding target pixels in the binary image obtained from CFAR detector are generally not capable of forming a connected region and may be separated into several parts. Thus, it is necessary to cluster target pixels in the binary image.

We suppose that the real length and width of the target of interest are L and W, respectively. Both the range and cross-range resolution of the image are ΔA. In fact, the area represented by target pixels is usually smaller than that of the real target; thus, the number of target pixels or the size of the target region detected by a CFAR detector has a superior value $S_{\max}$, namely,

$$S \leq S_{\max} = L \times W/(\Delta A \times \Delta A). \tag{14}$$

Moreover, the distance between pixels i and j within the same target region, denoted by $d(i,j)$, satisfies the following:

$$d(i,j) \leq d_{\max} = \sqrt{L^2 + W^2}/\Delta A. \tag{15}$$

Accordingly, we use the following flow shown in Fig. 3 to cluster target pixels in the binary image obtained after detection.

As we can see from the last step of the flow in Fig. 3, after the previous process, there still exist smaller regions or larger regions in the image, which are obviously unsuitable for the size of a target region. These undesired regions will certainly cause false alarms. In order to simplify the successive process, these regions are eliminated. The steps in detail are as follows: First, scanning the whole image, for every labeled region after clustering, we count the bright pixels in the region. Then, we remove the regions whose areas do not match the target's area range $\mathbf{S}_T = \{S | S_{\min} \leq S \leq S_{\max}\}$, where $S_{\max}$ is obtained from (14) and $S_{\min}$ is determined empirically.

IV. Fast Algorithm

The same as all the other CFAR algorithms for target detection using sliding window, the target detection algorithm shown in Fig. 1 also has the limitation of great computational complexity for parameter estimation in the local sliding window, when the size of window is large, which limits the practicability of the algorithm [6], [22].

Further investigating on the presented algorithm, we can find out that computing the global threshold and the index matrix is much less time consuming than the successive CFAR detecting process. Hence, we should first consider designing the fast CFAR algorithm.

Most running time of the CFAR algorithm is cost on parameter estimation in each sliding window [6], [22]. In fact, when scanning the whole image, the sliding window moves right or down by one pixel, and the corresponding two sliding windows centered at two adjacent test cells are largely overlapped. Take the moving-right case for example. As shown in Fig. 4, consider two test cells $I_{0\text{left}}$ and $I_{0\text{right}}$, which are adjacent to each other in the horizontal direction. When the center of the sliding window moves from $I_{0\text{left}}$ to $I_{0\text{right}}$, the left h pixels in the sliding window of $I_{0\text{left}}$ move out, and the right h pixels in the sliding window of $I_{0\text{right}}$ move in. Moreover, $N_C - h$ pixels

remain unchanged. The statistical values of these unchanged pixels have been used for the parameter estimation in the sliding window of $I_{0\text{left}}$; thus, reusing them in the sliding window of $I_{0\text{right}}$ will necessarily increase the computational burden. In Fig. 4, the size of r is selected to ensure enough clutter pixels for clutter statistics estimation. The guard area with width of $(h-2r)/2$ exists so that the clutter pixels are collected some distance away from the test cell and target pixels are prohibited from contaminating clutter statistics estimation. Let the real length and width of the interested target be L and W (suppose $L > W$), respectively; then $(h-2r)/2 > L/\Delta A$, where both the range and cross-range resolutions of the image are ΔA.

For the convenience of analyzing the computational complexity of the algorithm and designing the fast algorithm, we make the following simplifications.

1) Consider the extreme case. Suppose that the proposed CFAR detector is free of the censoring process, which means that all the clutter pixels in the sliding window contribute to parameter estimation. Then, there would be greater computational complexity compared with the process with censoring that only parts of the clutter pixels in the sliding window are used for parameter estimation. This is the worst case of the proposed algorithm proposed.
2) We take the example of the single-look image to analyze the computational complexity. Because the parameter estimations for multilook and single-look images only differ in the number of looks, the analysis of computational complexity and the design of fast algorithm for single-look images are also suitable for multilook images.
3) The analysis for the case of the sliding window moving from top to bottom is just the same as the case of the sliding window moving from left to right.

A. Design of Fast Algorithm

We can see from (10) and (11) that two variables are needed for the parameter estimation of the statistical distribution, namely, the mean of clutter intensity $E(I)$ and the mean of the square of the clutter intensity $E(I^2)$. Let μ_{left} and λ_{left} be the intensity mean and the mean of the square of the intensity of the clutter pixels in the sliding window of $I_{0\text{left}}$, respectively. Correspondingly, let μ_{right} and λ_{right} be the intensity mean and the mean of the square of the intensity of the clutter pixels in the sliding window of $I_{0\text{right}}$, respectively. Then, the relations between these variables are as follows:

$$\mu_{\text{right}} = \frac{N_C \cdot \mu_{\text{left}} - \sum_{i=1}^{h} I_i + \sum_{i=1}^{h} I'_i}{N_C} \tag{16}$$

$$\lambda_{\text{right}} = \frac{N_C \cdot \lambda_{\text{left}} - \sum_{i=1}^{h} I_i^2 + \sum_{i=1}^{h} I_i'^2}{N_C} \tag{17}$$

where N_C is the number of all the clutter pixels in the sliding window, and h is the height or width of the square sliding window. $\sum_{i=1}^{h} I_i$ denotes the sum of the intensity of the clutter pixels in the left column of the sliding window of $I_{0\text{left}}$. $\sum_{i=1}^{h} I'_i$ represents the sum of the intensity of the clutter pixels in the right column of the sliding window of $I_{0\text{right}}$. $\sum_{i=1}^{h} I_i^2$ is the sum of the square of the intensity of the clutter pixels in the left column of the sliding window of $I_{0\text{left}}$. $\sum_{i=1}^{h} I_i'^2$ is the sum of the square of the intensity of the clutter pixels in the right column of the sliding window of $I_{0\text{right}}$.

Hence, except the first test cell in the image, for all the other horizontally adjacent test pixels, μ_{right} and λ_{right} can be obtained by μ_{left} and λ_{left} according to (16) and (17). Thus, during the process of the sliding window scanning the image, posterior estimation can be obtained by the previous estimation. This result is significant for reducing computational load.

B. Analysis of the Computational Complexity for the Fast Algorithm

As for the first test cell in the image, combining Fig. 4 with (10) and (11), $N_C - 1$ multiplications and one addition are needed for computing μ, and $N_C + 1$ multiplications and $N_C - 1$ additions for λ. Thus, two multiplications and two additions are needed for $\hat{\alpha}$, while one multiplication and one addition for $\hat{\gamma}$. Hence, for the first test cell, a total of $N_C + 5$ multiplications and $2N_C + 1$ additions are needed. If the time of performing a multiplication and that of performing an addition are equal, there are a total of $3N_C + 6$ operations.

For all the other test cells except the first test cell, the parameter estimation of the clutter pixels in the sliding window of a test cell can be obtained by the statistics of its left adjacent pixel. Suppose the size of the image is $N \times N$, according to (16) and (17), the computational complexity of parameter estimation for the other $N^2 - 1$ test cells is shown in Table I ($\sum_{i=1}^{h} I_i$ and $\sum_{i=1}^{h} I_i^2$ have been obtained when computing μ_{left} and λ_{left}).

Assuming that the time of performing one multiplication and that of performing one addition are equal, the parameter estimation for the $N^2 - 1$ test cells needs $(N^2-1)(3h+12)$ operations in all. Thus, when the operation for the first pixel is added, the whole image needs altogether $(N^2-1)(3h+12) + 3N_C + 6$ operations.

C. Comparison With Other Algorithm on Computational Complexity

In order to evaluate the performance of the proposed algorithm quantitatively, we take performance comparisons among the fast algorithm mentioned earlier, the worst case of the proposed algorithm without fast computational strategy, and the widely used two-parameter CFAR detector proposed by Lincoln Laboratory. The worst case of the proposed algorithm without fast computational strategy and the Salazar algorithm has equal computational complexity. The computational-complexity analysis of the Salazar algorithm and the two-parameter CFAR algorithm are given in Table II and Table III, respectively. $N^2(3N_C + 6)$ operations are needed for the parameter estimation of the whole image by the Salazar algorithm and $N^2(3N_C + 2)$ operations by the two-parameter CFAR algorithm. Based on the aforementioned comparison, there is no

TABLE I
COMPUTATIONAL COMPLEXITY OF ESTIMATING THE PARAMETERS FOR ALL THE OTHER TEST CELLS EXCEPT FOR THE FIRST TEST PIXEL

The fast algorithm proposed	for each tested cell, Computing μ	for each test cell, Computing λ	For each test cell, Computing $\hat{\alpha}$	for each test cell, Computing $\hat{\gamma}$	For the N^2-1 pixels left, sum total
Addition (times)	$h+1$	$h+1$	2	1	$\left(N^2-1\right)\left(2h+5\right)$
Multiplication (times)	2	$h+2$	2	1	$\left(N^2-1\right)\left(h+7\right)$

TABLE II
COMPUTATIONAL COMPLEXITY ANALYSIS OF THE SALAZAR ALGORITHM (THE WORST CASE WITHOUT USING THE FAST ALGORITHM)

The Salazar algorithm	for each test cell, Computing μ	for each test cell, Computing λ	for each test cell, Computing $\hat{\alpha}$	for each test cell, Computing $\hat{\gamma}$	sum total
Addition (times)	N_C-1	N_C-1	2	1	$N^2\left(2N_C+1\right)$
Multiplication (times)	2	$h+2$	2	1	$\left(N^2-1\right)\left(h+7\right)$

TABLE III
COMPUTATIONAL COMPLEXITY ANALYSIS OF THE TWO-PARAMETER CFAR ALGORITHM

The Two-parameter CFAR algorithm	Computing each pixel	Computing the variance of each pixel	sum total
Addition(times)	N_C-1	N_C	$N^2\left(2N_C-1\right)$
Multiplication (times)	1	N_C+2	$N^2\left(N_C+3\right)$

significant difference of the computational complexity between the Salazar and two-parameter CFAR algorithms. Based on the simplifications mentioned in Section IV, Table I gives the worst performance of the proposed fast algorithm. Hence, the ratio of the computational complexity of the Salazar algorithm to that of the proposed algorithm is at least

$$\tau_1 > \frac{N^2(3N_C+6)}{(N^2-1)(3h+12)+3N_C+6} \approx \frac{N^2(3N_C+6)}{N^2(3h+12)} \approx \frac{N_C}{h} \approx 4r. \tag{18}$$

The ratio of the computational complexity of the two-parameter CFAR algorithm to that of the proposed algorithm is at least

$$\tau_2 > \frac{N^2(3N_C+2)}{(N^2-1)(3h+12)+3N_C+6} \approx \frac{N^2(3N_C+2)}{N^2(3h+12)} \approx \frac{N_C}{h} \approx 4r \tag{19}$$

where r is the width of the reference sliding window shown in Fig. 4.

Equations (18) and (19) indicate that the computational complexities of the Salazar and two-parameter CFAR algorithms are, respectively, at least $4r$ times that of the proposed algorithm no matter how large is the image size. When the width of the sliding window is the smallest, i.e., $r=1$, τ_1 and τ_2 have the inferior value of four, namely, the computational complexities of the Salazar and two-parameter CFAR algorithms are, respectively, at least four times that of the proposed algorithm. Generally speaking, in order to evaluate the statistical performance of the clutter accurately, the width of the reference sliding window is usually much larger; therefore, both τ_1 and τ_2 increase greatly. Accordingly, the proposed fast algorithm does significantly improve the computational efficiency theoretically.

V. ALGORITHM PERFORMANCE ANALYSIS

In this section, theoretical analysis is given to show the performance of the proposed algorithm. For the sake of simplicity, we consider the single-look clutter environment (the conclusions for the single-look case can be extended to the multilook case) and the ideal case that the target intensity fluctuation follows a negative-exponential distribution [5]. According to (8) and (9), the false alarm probability of the detector is obtained by

$$p_{\text{fa}} = 1 - \int_0^{T_l} \frac{-\alpha\gamma^{-\alpha}}{(\gamma+I)^{1-\alpha}}\, dI = \left(\frac{T_l}{\gamma}+1\right)^{\alpha}. \tag{20}$$

The detection probability is

$$p_d = \frac{1}{\sigma_T}\int_{T_l}^{\infty} \exp\left[-\frac{I}{\sigma_T}\right]\, dI = \exp\left[-\frac{T_l}{\sigma_T}\right] \tag{21}$$

where σ_T is the mean value of the negative-exponential distribution, and it denotes the power level of the target. Using

(11) and (12), and let signal-to-clutter ratio (SCR) be SCR $= \sigma_T/\sigma_B$ (σ_B is the average value of clutter intensity), then we rewrite (21) as

$$p_d = \exp\left\{\frac{(\alpha+1)\left(p_{\mathrm{fa}}^{1/\alpha}-1\right)}{\mathrm{SCR}}\right\}. \tag{22}$$

Equation (22) shows that the detection probability of the algorithm is closely related to the clutter environment (related by the degree of homogeneity α) surrounding the targets and the SCR under the condition that the false alarm probability is given. This coincides with our intuitive understanding. Given $p_{\mathrm{fa}} = 10^{-3}$, Fig. 5 shows the performance curves of target detection with different clutter situations and SCR values. In Fig. 5(a) and (b), it can be seen that, with a fixed α, the target detection probability increases as SCR increases. Moreover, the detection performance with a small α is notably better than that with a large α. The value of α denotes the clutter environment that the target detection is in face of. As for homogeneous clutter and clutter edge, the value of α is relatively smaller, while for multitarget situations, the value of α is relatively larger. Therefore, without the proposed censoring procedure, which is able to eliminate the influence of the interfering targets, the detection performance in multitarget situations is determined to degrade significantly in contrast with that in homogeneous clutter and clutter edge situations.

The aforementioned analysis indicates that, for the single-look case, the proposed algorithm and the Salazar algorithm exhibit the same detection performance in homogeneous clutter and clutter edge situations. As for multitarget situations, considering (22), intuitively, given false alarm probability p_{fa} in advance, due to the introduction of the censoring procedure, lots of relatively brighter interfering targets in clutter region are discarded. This directly leads to the change of two parameters. One is that the degree of homogeneity for the region increases due to the decrease of the abnormal target pixels in the clutter region, namely, the value of α decreases. Another is that the SCR for the test cell increases compared with that for clutter region. It is easy to observe from (22) that the increase of SCR or the decrease of α will cause an increase in detection probability. Moreover, this is the reason why we introduce censoring procedure to improve the detection performance in multitarget situations.

The previous analysis demonstrates that the SCR and the clutter homogeneity degree surrounding targets also increase as the censoring depth increases. However, one disadvantage is that, as the detection probability increases, the false alarm probability increases, too. This definitely brings some CFAR loss. For widely varying real scenes, CFAR loss is influenced by many factors. Hence, it is unable to theoretically deduce the relation between CFAR loss and the censoring depth. Still, from the flow of the proposed algorithm, it can be noted that the proposed algorithm has a great ability to control the false alarm rate. First, the proposed algorithm performs robustly over an error range of the censoring depth. The reason is that the interfering target pixels are brighter and they contribute to the tail of the histogram of SAR images. Although the

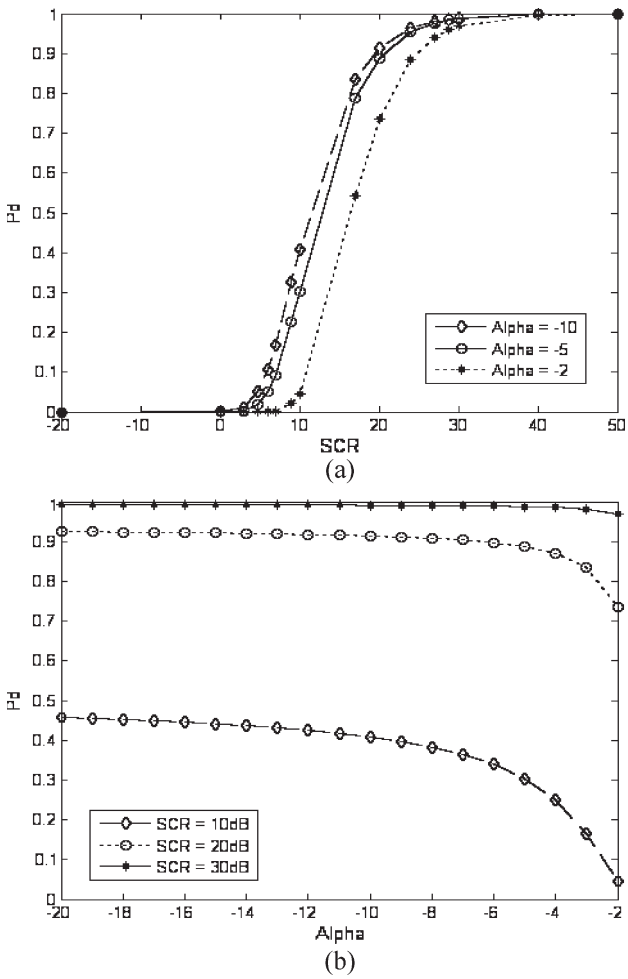

Fig. 5. Detection performance with different SCRs and clutter situations. (a) Curves of Pd versus SCR. (b) Curves of Pd versus α.

global threshold (decided by the censoring depth) varies over a wide range corresponding to the tailed part of the histogram, abnormal target pixels censored have slight changes, and their influence on the statistical characteristic of most local clutter regions is limited. Hence, there is a wide range for the proper selection of the global threshold. When the global threshold is within this range, the proposed algorithm exhibits good detection performance. As a result, this allows the selection of the global threshold and the censoring depth not to be so exact. Second, clustering procedure further reduces the false alarm rate.

VI. Experimental Results and Analysis

Fig. 6(a) shows an airborne X-band HH polarization single-look SAR image of some region in Beijing, with a resolution of 0.5 $\times$ 0.5 m and a size of 200 $\times$ 500 pixels. Fig. 6(b) shows a sketch of Fig. 6(a). The left part of the image shown in Fig. 6(a) is the concrete runway, and the right part is grass. Small trees are spreading in the grass. At the border of the grass and the concrete runway, namely, the clutter edge, there is bush. To the left of the bush, there are some small concrete blocks which are arranged with equidistance and connected by iron fence. Fig. 6(c) shows an optical photograph of the clutter

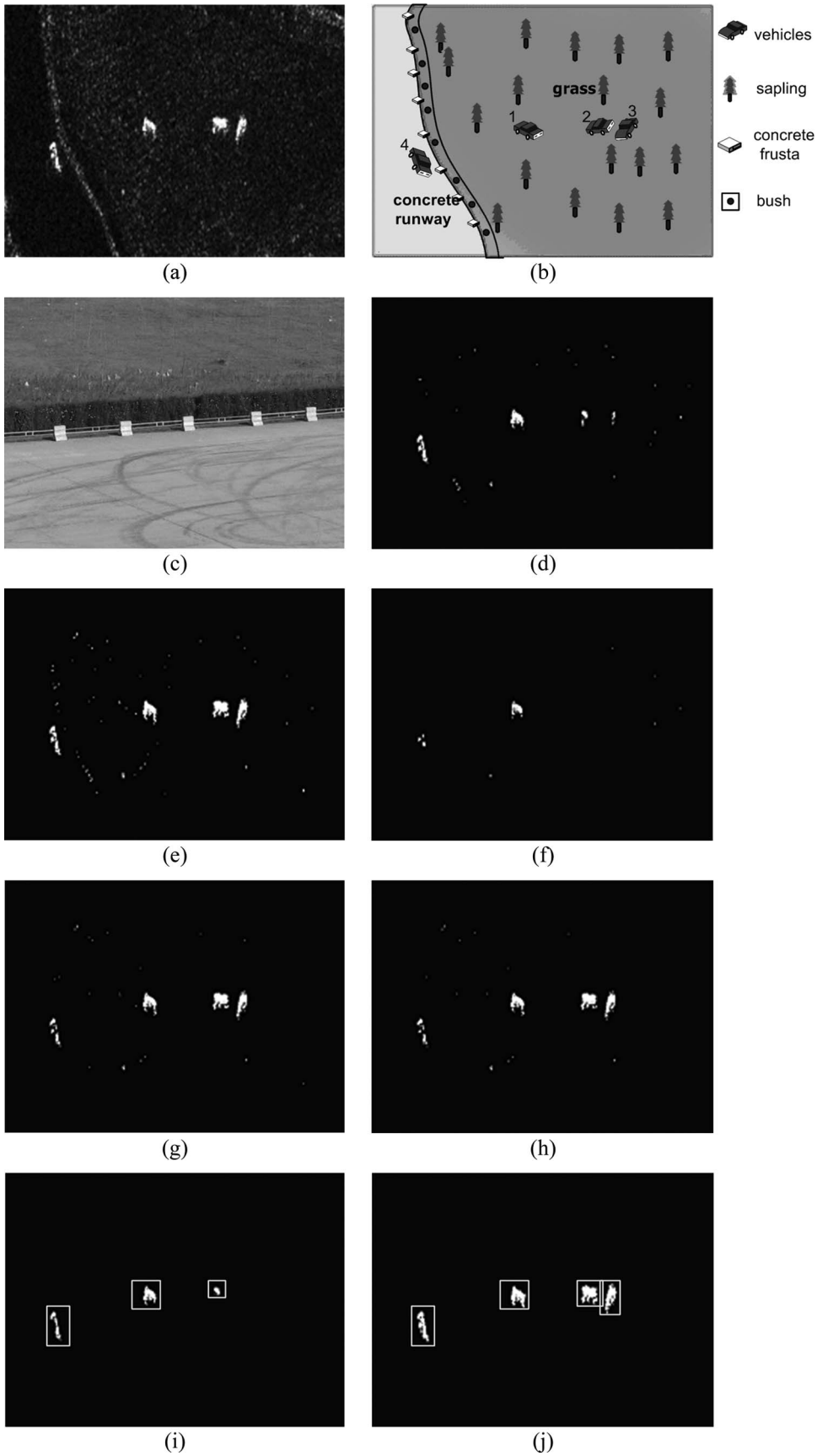

Fig. 6. Results of target detection for a typical SAR scene. (a) Original SAR image. (b) Illustration of scene content. (c) Optical photo corresponding to clutter edge. (d) Detection result of the Salazar algorithm with $p_{\mathrm{fa}} = 10^{-3}$. (e) Detection result of the proposed algorithm with $p_{\mathrm{fa}} = 10^{-3}$. (f) Detection result of the Salazar algorithm with $p_{\mathrm{fa}} = 10^{-4}$. (g) Detection result of the proposed algorithm with $p_{\mathrm{fa}} = 10^{-4}$. (h) Detection result of the proposed algorithm with $p_{\mathrm{fa}} = 10^{-5}$. (i) Clustering result of (d). (j) Clustering result of (e).

edge area. There are also tanks in the scene, numbered 1–4. The surrounding of target 1 is grass area, the distance between targets 2 and 3 is very small (denotes the multitarget situation), and target 4 is located at the clutter edge. The scene shown in Fig. 6(a) is a typical type of scene which can be used to evaluate the performance of detection algorithm completely.

Salazar has made conclusions [8] that the mismatch of the clutter modeling results in great CFAR loss, which accounts for that the Salazar algorithm outperforms the conventional two-parameter CFAR detector. Thus, we only compare the proposed CFAR algorithm with the Salazar algorithm. Fig. 6(d) shows the detection results by the Salazar algorithm given the theoretical false alarm probability $p_{\mathrm{fa}} = 10^{-3}$. Correspondingly, Fig. 6(e) shows the results by the proposed algorithm given the same false alarm probability. Fig. 6(f) shows the detection results by the Salazar algorithm given $p_{\mathrm{fa}} = 10^{-4}$. Fig. 6(g) and (h) shows the results by the proposed algorithm given $p_{\mathrm{fa}} = 10^{-4}$ and $p_{\mathrm{fa}} = 10^{-5}$, respectively.

We take both the resolution and the practical size of target into consideration. In order to prevent the test target pixels leaking into the clutter region of the corresponding sliding window, Fig. 6(d)–(h) shows the results of selecting square sliding window with length of $h = 71$, the ring window with length of 31, and the annular area with width $r = 20$. These parameters are fixed for the entire image. The global threshold T_g for the proposed algorithm is obtained with a confidence level of $1 - \varphi = 90\%$. Comparing the results in Fig. 6(d) and (e), given the same theoretical false alarm probability for both algorithms, for detecting target 1 in homogenous clutter area and target 4 in clutter edge area, we can see that both the proposed algorithm and the Salazar algorithm have comparatively good detection results and the derived target contours are complete and clear. Whereas for multitarget situation, e.g., for targets 2 and 3, which are close to each other, the proposed algorithm obviously outperforms the Salazar algorithm. Since the clutter statistics estimation is influenced by the adjacent target pixels, only a few pixels of targets 2 and 3 are detected by the Salazar algorithm with much information lost, while the two close targets are well detected by the proposed algorithm. In other words, the proposed algorithm also has better performance for target detection in multitarget situation.

With comparisons between Fig. 6(d) and (e), we can find out that, although the proposed algorithm does better in detecting targets, there are relatively more "small areas" in the image. These small areas, mainly brought about by the concrete blocks with relatively strong backscattering, most concentrate in the clutter edge between the concrete runway and the grass.

Fig. 6(f)–(h) shows that, given the theoretical false alarm probability $p_{\mathrm{fa}} = 10^{-4}$, using the Salazar algorithm, the closely located two targets are both undetected and the information of the target located in the homogeneous area and the clutter edge are lost to more or less extent, while the proposed algorithm can keep much more target information, and the results are much better. These results strongly illustrate that the proposed CFAR algorithm significantly outperforms the Salazar algorithm.

In order to make further comparisons between the Salazar algorithm and the proposed algorithm, suppose that the target pixels are those pixels with values larger than the global threshold value T_g. If the number of all these target pixels is $N_{t\arg et}$ and the size of the image is $N \times M$, then the number of clutter pixels in the image is $N_{\mathrm{clutter}} = N \times M - N_{t\arg et}$. The number of target pixels detected is N_{dt}, and the number of false alarm pixels is N_{dc}. Then, the actual detection ratio is defined as

$$P_d = \frac{N_{dt}}{N_{t\arg et}}. \tag{23}$$

The actual false alarm ratio is

$$P_f = \frac{N_{dc}}{N_{\mathrm{clutter}}}. \tag{24}$$

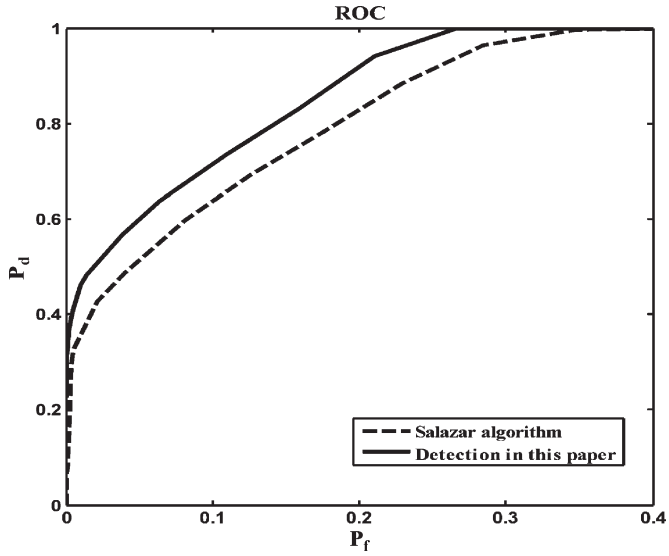

Fig. 7. Comparison of the ROC curves of two algorithms.

As shown in Fig. 7, combining (23) with (24), we get the receiver operating characteristic (ROC) curves of the Salazar and proposed CFAR algorithms. These curves indicate that the proposed CFAR algorithm has better performance than the Salazar algorithm.

Fig. 6(i) and (j) shows the results of targets clustering from Fig. 6(d)–(e), respectively. The inferior threshold for removing areas is 30. As shown in Fig. 6(d), the result of the Salazar algorithm for detecting the closely located two targets is poor, and much information of targets is lost after CFAR detection. Target 3 is taken as clutter false alarms and removed during the process of area removing. However, all the four targets are detected by the proposed algorithm.

To sum up, taking the case with $p_{\mathrm{fa}} = 10^{-3}$, for example, we give the integrative comparisons of the final detection results by the Salazar algorithm followed by targets clustering and by the proposed algorithm shown in Fig. 2. The results are shown in Table IV. All the experiments are accomplished by nonoptimized Matlab codes with a hardware environment of PIII 500M CPU and 512M memory. In view of time consuming, Salazar algorithm and the proposed algorithm without using fast algorithm nearly have equal running time. However, by using fast algorithm, the consumed time is only 1.6398s,

TABLE IV
WHOLE PERFORMANCE COMPARISONS BETWEEN THE TWO ALGORITHMS: $p_{\mathrm{fa}} = 10^{-3}$

	Number of all the targets	Number of detected targets	False alarms	Running time (s)	
The Salazar algorithm	4	3	0	100.5469	
The proposed algorithm	4	4	0	Common algorithm	102.1719
				Fast algorithm	1.6398

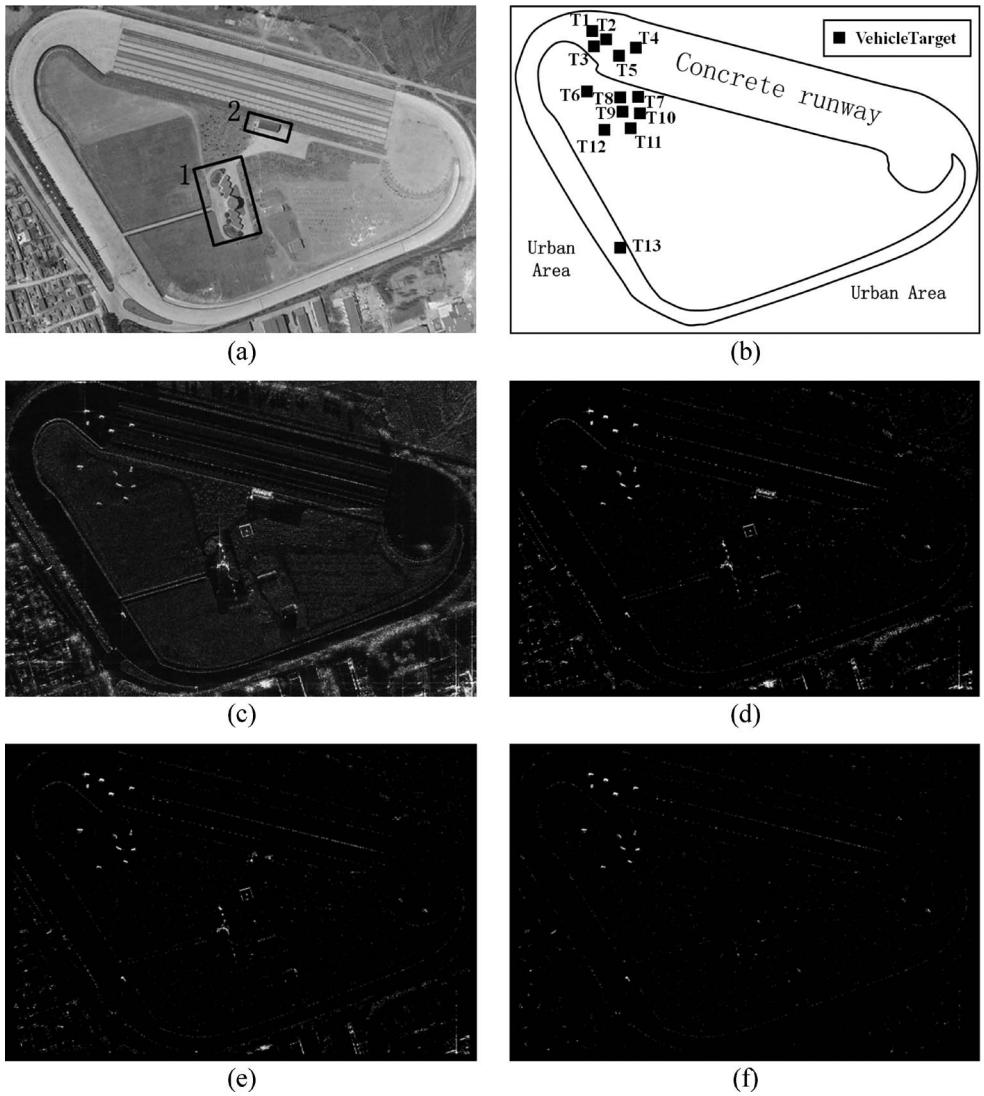

Fig. 8. Results of target detection from an urban SAR scene. (a) Optical photograph of a test scene without targets. (b) Location index of 13 targets (T1–T13). (c) SAR image of the scene with targets. (d) Detection result of the proposed algorithm with $p_{\mathrm{fa}} = 10^{-3}$ and $1 - \varphi = 95\%$. (e) Detection result of the proposed algorithm with $p_{\mathrm{fa}} = 10^{-3}$ and $1 - \varphi = 99\%$. (f) Detection result of the Salazar algorithm with $p_{\mathrm{fa}} = 10^{-3}$.

which is 1/61 of the time by Salazar algorithm and 1/62 of the time by the proposed algorithm without fast strategy. Theoretically, by using the proposed fast algorithm in the period of estimating parameters, which is the main time-consuming process, the computational speed of the proposed fast algorithm should be $4r = 80$ (the width of the annular window is $r = 20$) times as fast as that by using the Salazar algorithm. Taking account of the compiling time of Matlab itself and the time consumed for comparison with the global threshold, the performance of the fast algorithm is in accord with the theoretical analysis.

Aside from Fig. 6, we give some more results of real SAR images to evaluate the proposed algorithm. Fig. 8 shows another test SAR image containing vehicles in a complex urban clutter setting, which is collected in 2005. The airborne SAR platform operated at X-band and collected the data in stripmap mode

HH polarization, with a resolution of 0.5 m both in range and in cross-range.

Fig. 8(a) shows an optical (ground truth) photograph of the scene used in this paper. As we can see, there are a lot of trees and buildings but no vehicle target. The objects numbered 1 and 2 are two typical buildings in Fig. 8(a). According to Fig. 8(b), the left-bottom and right-bottom parts of the image shown in Fig. 8(a) are urban areas. There is a concrete runway in Fig. 8(a). Fig. 8(c) shows the corresponding SAR image of this scene placed with 13 military vehicles shown in Fig. 8(b). The image size is 1375×1880 pixels.

We use the same sliding window as the processing of Fig. 6. Fig. 8(d) shows the detection results by the proposed algorithm with the theoretical false alarm probability $p_{\text{fa}} = 10^{-3}$ and the censoring depth $1 - \varphi = 95\%$. Correspondingly, Fig. 8(e) shows the results by the proposed algorithm with the same false alarm probability and the censoring depth $1 - \varphi = 99\%$. Fig. 8(f) shows the detection results by the Salazar algorithm with $p_{\text{fa}} = 10^{-3}$.

Comparing the results in Fig. 8(d)–(f), given the same theoretical false alarm probability for both algorithms, for detecting targets T1–T12 in homogenous clutter area and target T13 in clutter edge area, we can see that both the proposed algorithm and the Salazar algorithm have comparatively good detection results and the derived target contours are complete and clear. Whereas for buildings numbered 1 and 2 and the urban areas which can be denoted as multitarget situation, the proposed algorithm outperforms the Salazar algorithm. Since the clutter statistics estimation is influenced by the adjacent target pixels, few pixels of buildings numbered 1 and 2 and the urban areas are detected by the Salazar algorithm with much information lost, while they are well detected by the proposed algorithm although the censoring depth varies from 95% to 99%. In other words, the proposed algorithm also has better performance for target detection in multitarget situation.

All the experiments are accomplished by the same Matlab codes and the same hardware environment as the processing of Fig. 6. In view of time consuming, Salazar algorithm and the proposed algorithm without using fast algorithm nearly have equal running time. The proposed algorithm is 42.3168 min, whereas the Salazar algorithm is 41.6014 min. However, by using fast algorithm, the consumed time is only 40.0471 s, which is 1/62.3287 of the time by Salazar algorithm and 1/63.4005 of the time by the proposed algorithm without fast strategy. Taking account of the compiling time of Matlab itself and the time consumed for comparison with the global threshold, the performance of the fast algorithm is in accord with the theoretical analysis.

VII. Conclusion

An adaptive and fast CFAR algorithm based on AC is proposed in this paper. First, an adaptive global threshold is used to acquire the index matrix that labels whether it is a potential target pixel or not for each pixel in the image. Then, the clutter pixels in the sliding window of detection process are censored automatically by the index matrix in order to decide the clutter environment of detection adaptively. The G^0 distribution, which can model multilook SAR images within an extensive range of degree of homogeneity, is introduced to describe the statistical characteristic of clutter. With the additional process of the AC, the detector has CFAR characteristic and good performance when detecting target in homogeneous regions, the clutter edge, and multitarget situations. Simultaneously, the corresponding fast algorithm can greatly reduce the computational load. Finally, the more accurate extraction of target regions can be obtained by target clustering process. The experimental results of the typically real SAR scene validate the effectiveness of the proposed algorithm.

References

[1] D. E. Dudgeon and R. T. Lacoss, "An overview of automatic target recognition," *Linc. Lab. J.*, vol. 6, no. 1, pp. 3–10, 1993.

[2] T. D. Ross, J. J. Bradley, L. J. Hudson, and M. P. O'Connor, "SAR ATR: So what's the problem? An MSTAR perspective," in *Proc. SPIE Conf. Algorithms SAR Imagery IV*, Orlando, FL, 1999, vol. 3721, pp. 662–672.

[3] B. Bhanu, D. E. Dudgeon, E. G. Zelnio, A. Rosenfeld, D. Casasent, and I. S. Reed, "Guest editorial introduction to the special issue on automatic target detection and recognition," *IEEE Trans. Image Process.*, vol. 6, no. 1, pp. 1–6, Jan. 1997.

[4] L. M. Novak, G. J. Owirka, and W. S. Brower, "An efficient multi-target SAR ATR algorithm," in *Proc. IEEE 32nd* Asilomar Conf. Signals, Syst., Comput., 1998, vol. 1, pp. 3–13.

[5] C. J. Oliver and S. Quegan, *Understanding Synthetic Aperture Radar Images*. Boston, MA: Artech House, 1998.

[6] L. M. Novak and S. R. Hesse, "On the performance of order-statistics CFAR detectors," in *Proc. IEEE 25th* Asilomar Conf. Signals, Syst., Comput., 1991, vol. 2, pp. 835–840.

[7] M. di Bisceglie and C. Galdi, "CFAR detection of extended objects in high-resolution SAR images," *IEEE Trans. Geosci. Remote Sens.*, vol. 43, no. 4, pp. 833–843, Apr. 2005.

[8] J. S. Salazar, II, "Detection schemes for synthetic aperture radar imagery based on a beta prime statistical model," Ph.D. dissertation, Univ. New Mexico, Albuquerque, NM, 1999.

[9] L. M. Novak, G. J. Owirka, W. S. Brower, and A. L. Weaver, "The automatic target-recognition system in SAIP," *Linc. Lab. J.*, vol. 10, no. 2, pp. 187–202, 1997.

[10] R. A. English, S. J. Rawlinson, and N. M. Sandirasegaram, "Development of an ATR workbench for SAR imagery," De Defense R&D, Ottawa, ON, Canada, Tech. Rep., DRDC Ottawa, TR2002-155, 2002.

[11] S. Kuttikkad and R. Chellappa, "Non-Gaussian CFAR techniques for target detection in high resolution SAR images," in *Proc. ICIP*, 1994, vol. 1, pp. 910–914.

[12] M. E. Smith and P. K. Varshney, "VI-CFAR: A novel CFAR algorithm based on data variability," in *Proc. IEEE Nat. Radar Conf.*, Syracuse, NY, 1997, pp. 263–268.

[13] M. E. Smith and P. K. Varshney, "Intelligent CFAR processor based on data variability," *IEEE Trans. Aerosp. Electron. Syst.*, vol. 36, no. 3, pp. 837–847, Jul. 2000.

[14] X. Huang, H. Sun, W. Luo, X. Xu, and W. Yang, "Intelligent CFAR detector based on region classification for SAR images," *J. Wuhan Univ. (Nat. Sci. Ed.)*, vol. 50, no. 1, pp. 104–108, 2004.

[15] X. L. Fang, "Target detection and discrimination in UWB-SAR image," Ph.D. dissertation, Nat. Univ. Defense Technol., Changsha, China, 2005.

[16] A. Farrouki and M. Barkat, "Automatic censoring CFAR detector based on ordered data variability for nonhomogeneous environments," *Proc. Inst. Elect. Eng.—Radar, Sonar Navig.*, vol. 152, no. 1, pp. 43–51, Feb. 2005.

[17] M. D. Bisceglie and C. Galdi, "CFAR detection of extended objects in high resolution SAR images," in *Proc. IGARSS*, 2001, vol. 6, pp. 2674–2676.

[18] J. T. Rickard and G. M. Dillard, "Adaptive detection algorithms for multiple-target situations," *IEEE Trans. Aerosp. Electron. Syst.*, vol. AES-13, no. 4, pp. 338–343, Jul. 1977.

[19] A. C. Frery, H. J. Muller, C. C. F. Yanasse, and S. J. S. Sant'Anna, "A model for extremely heterogeneous clutter," *IEEE Trans. Geosci. Remote Sens.*, vol. 35, no. 3, pp. 648–659, May 1997.

[20] H. X. Zhou, "The research of detecting ship target and ship wake from SAR imagery," Ph.D. dissertation, Nat. Univ. Defense Technol., Changsha, China, 2003.
[21] F. X. Hofele, "An innovative CFAR algorithm," in *Proc. CIE Int. Conf. Radar*, 2001, pp. 329–333.
[22] G. Gao, G. Kuang, Q. Zhang, and D. Li, "Fast detecting and locating groups of targets in high-resolution SAR images," *Pattern Recognit.*, vol. 40, no. 4, pp. 1378–1384, Apr. 2007.
[23] M. S. Greco and G. Gini, "Statistical analysis of high-resolution SAR ground clutter data," *IEEE Trans. Geosci. Remote Sens.*, vol. 45, no. 3, pp. 566–575, Mar. 2007.
[24] G. Moser, J. Zerubia, and S. B. Serpico, "Dictionary-based stochastic expectation–maximization for SAR amplitude probability density function estimation," *IEEE Trans. Geosci. Remote Sens.*, vol. 44, no. 1, pp. 188–200, Jan. 2006.
[25] Y. Delignon and W. Pieczynski, "Modeling non-Rayleigh speckle distribution in SAR images," *IEEE Trans. Geosci. Remote Sens.*, vol. 40, no. 6, pp. 1430–1435, Jun. 2002.
[26] C. Tison, J. M. Nicolas, F. Tupin, and H. Maitre, "A new statistical model for Markovian classification of urban areas in high-resolution SAR images," *IEEE Trans. Geosci. Remote Sens.*, vol. 42, no. 10, pp. 2046–2057, Oct. 2004.
[27] P. Mantero, G. Moser, and S. B. Serpico, "Partially supervised classification of remote sensing images through SVM-based probability density estimation," *IEEE Trans. Geosci. Remote Sens.*, vol. 43, no. 3, pp. 559–570, Mar. 2005.
[28] A. Achim, E. E. Kuruoglu, and J. Zerubia, "SAR image filtering based on the heavy-tailed Rayleigh model," *IEEE Trans. Image Process.*, vol. 15, no. 9, pp. 2686–2693, Sep. 2006.

Gui Gao received the B.S. degree in information engineering and the M.S. and Ph.D. degrees in remote sensing information processing from the National University of Defense Technology, Changsha, China, in 2002, 2004, and 2007, respectively.

He is currently an Associate Professor with the School of Electronic Science and Engineering, National University of Defense Technology. He is the author of over 50 papers. His research interests include synthetic aperture radar automatic target recognition, statistical modeling of SAR image, and data mining.

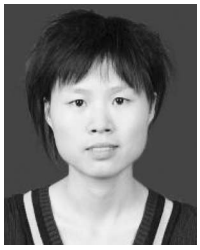

Li Liu received the B.S. degree in communication engineering and the M.S. degree in remote sensing and geographic information system from the National University of Defense Technology, Changsha, China, in 2003 and 2005, respectively, where she is currently working toward the Ph.D. degree.

She is currently a Visiting Student at the University of Waterloo, Waterloo, ON, Canada. Her current research interests include SAR image texture classification and Markov random field techniques.

Lingjun Zhao received the B.S. degree in information engineering and the M.S. degree in circuits and system from the National University of Defense Technology, Changsha, China, in 2003 and 2004, respectively, where she is currently working toward the Ph.D. degree.

Her current research interests include synthetic aperture radar (SAR) image classification and urban SAR image interpretation, particularly automatic object (buildings, road, etc.) extraction from urban areas.

Gongtao Shi received the B.S. and M.S. degrees in communication engineering from Air Force Engineering University, Xi'an, China, in 2003 and 2006, respectively. He is currently working toward the Ph.D. degree at the National University of Defense Technology, Changsha, China.

His current research interests include synthetic aperture radar (SAR) image processing and SAR ground moving target indication.

Gangyao Kuang received the B.S. and M.S. degrees from the Central South University of Technology, Changsha, China, in 1988 and 1991, respectively, and the Ph.D. degree from the National University of Defense Technology, Changsha, in 1995.

Since 1996, he has been the Codirector of the Remote Sensing Information Processing Laboratory, National University of Defense Technology, where he has worked on synthetic aperture radar (SAR) signal and image processing, automatic target detection and recognition, information fusion, and various remote sensing projects. He is currently a Professor in the School of Electronic Science and Engineering, National University of Defense Technology. He is the author/coauthor of over 200 papers and one book. His current interests include remote sensing, SAR image processing, change detection, SAR ground moving target indication, and the classification of polarimetric SAR images.